Available online at www.sciencedirect.com

ScienceDirect

Procedia Engineering 4 (2010) 35–50

Procedia Engineering

www.elsevier.com/locate/procedia

ISAB-2010

# Dynamic response and structural integrity of submerged floating tunnel due to hydrodynamic load and accidental load

Youshi Hong*, Fei Ge

*LNM, Institute of Mechanics, Chinese Academy of Sciences, Beijing 100190, China*

**Abstract**

This paper generally describes the research advances on dynamical response and structural integrity of submerged floating tunnel (SFT) subjected to hydrodynamic load and accidental load, which were accomplished by a research team in the Institute of Mechanics, Chinese Academy of Sciences in recent years. By means of theoretic analysis, modeling, calculation and experimental investigation, the research team has achieved creative results in several aspects including: (1) ABB Selection and its environmental & geotechnical conditions for ABP design, (2) Dynamic characteristics of SFT due to wave and current loads, (3) Effects of SFT structural parameters on its dynamic response, (4) Geotechnical investigations and tension pile analysis, (5) Dynamic response of SFT due to seismic load and accidental load, (6) Effects of water and sea-water on high-cycle and very-high-cycle fatigue behavior for metallic materials, and (7) Design of ABP of Qiandao Lake and its structure analysis & strength assessment.



*Keywords:* Submerged floating tunnel; hydrodynamic load; buoyancy-weight ratio; tension pile; seismic effect; corrosion fatigue; structural integrity; strength assessment

## 1. Introduction

Submerged floating tunnel (SFT) i.e. Archimedes Bridge is a kind of structural passage floating and submerged within water body to bridge two shores, which takes the advantage of buoyancy and is tethered to the foundation and the shore. Fig. 1(a) shows an SFT demonstration model in our laboratory. SFT is a new alternative solution for the crossing of sea strait, river, lake or other water sound with the water depth of 50 meters or more. As an innovative technique, it will become attractive competing with other traditional techniques with its economic and environmental advantages. At present, there is still not an actual SFT being built in the world. To build such a structure will encounter various technical problems and difficulties. These include structure type of the tunnel, tethering to the tunnel, anchoring to water-bed, installation, shore connection, etc. Water wave and current effect, earthquake effect and tsunami effect need to be investigated. Thus, experimental investigations and numerical

* Corresponding author. Tel.: +86-10-82543966; fax: +86-10-62561284.
*E-mail address*: hongys@imech.ac.cn.

1877-7058 © 2010 Published by Elsevier Ltd.
doi:10.1016/j.proeng.2010.08.006

simulations in laboratory may provide useful premise for the design and the preparation of construction. Another important step is to build an SFT prototype to show its feasibility for the world.

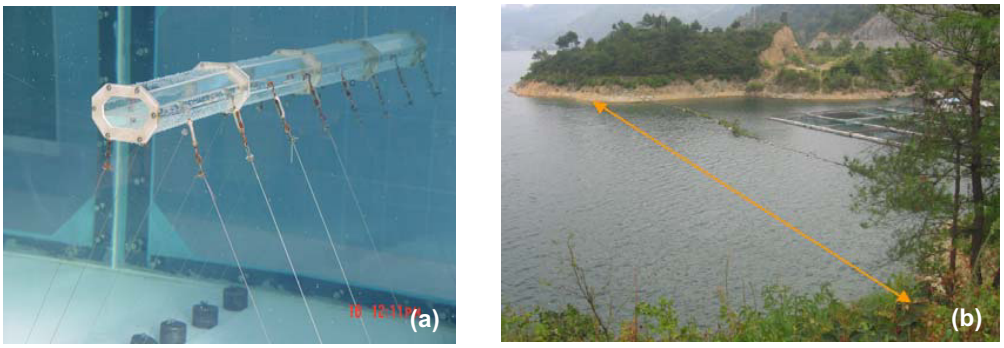


Fig. 1. (a) An SFT demonstration model in laboratory of IMECH; (b) West view of ABB, the line indicating the selected route for ABP

Since 1980s, there have been researches regarding SFT conceptual design and dynamic response by investigators from Italy, Norway, China, Japan, USA, etc. Brancaleoni et al. [1] first simulated the dynamic response of SFT with different mooring types. They suggested that the short-span tunnel with large buoyancy can provide stiffness to withstand severe environments, and when moored by cables, an initial sufficient tension should be given to avoid slackening phenomena. Remseth et al. [2] calculated the problem of two-dimensional hydrodynamics of SFT under regular waves. Their results indicated that the maximal response may occur for non-normal incidence of waves, and the introduction of short crested waves will reduce the directionality effects. Kanie et al. [3] and Kunisu et al. [4] analyzed the effect of waves on the dynamics of SFT under regular waves. They found when oblique angle of the incident wave increases, the wave force in the transverse direction decreases, whereas the wave force in the vertical direction stays constant. Kunisu et al. [5] performed experiments on two-dimensional model, investigating the dynamics of SFT subjected to the wave environment of Hokkaido. Their results showed, for the case of tether perpendicular to sea-bed, the transverse displacement is significant, but the snap force is almost negligible. Perotti et al. [6, 7] calculated the dynamic response due to wave and seismic loading for SFT in the conceptual design of Messina Strait. They noted that the flexible responses of short anchoring elements, excited by seismic loading, will yield inelastic behaviour, yet the dynamic responses due to wave loading is one order of magnitude smaller than those due to seismic loading. Kiyokawa et al. [8] and Morita et al. [9] calculated the effect of fluid compressibility on the SFT dynamics due to seismic excitation. They proposed that the influence of fluid compressibility cannot be ignored when the wave frequency is higher than 1 Hz. Venkataramana et al. [10] experimentally investigated the effect of flow velocity on the vibration of SFT in a water tank with one-dimension cyclic flow. The results pointed out the horizontal responses increase with flow velocity, whereas the variation in the vertical responses is much more complicated and susceptible to eddies and other forms of turbulence.

In China, several research groups from universities and research institutions have involved in SFT researches since late 1990s. The research teams from Zhejiang University, Tongji University and Institute of Mechanics (IMECH), Chinese Academy of Sciences (CAS) successively cooperated with Italian research teams engaged in the projects of “Feasibility Study of Jintang Strait SFT” [11, 12] and “Archimedes Bridge Prototype in Qiandao Lake” [13, 14]. The later project was implemented via Sino-Italian Laboratory of Archimedes Bridge (SIJLAB) between December 2004 and December 2009. Fig.1 (b) is the lake bay for the location of the Prototype. Xiang et al. [15, 16] completed the structural analysis for the SFT design in Jintang Strait, and performed model experiments. Ge et al. [17, 18], taking into account the excitation effect of tunnel tube on the tether and the irregularity of water current, calculated the nonlinear vortex-induced-vibration (VIV) of tethers, and analyzed the effect of buoyancy-weight ratio (BWR) on the VIV of SFT [19]. Ge et al. [20] also investigated the characteristics of cross-flow and in-line vibration of a cylinder with large aspect ratio (length to diameter) under uniform flow. Chen et al. [21, 22] modified the wake oscillator model so as to analyze the effects of tether tension and flow non-uniformity on tether VIV. Dong et al. [23, 24] performed structural analysis on curved SFT, especially analyzed the stress distribution of the structure induced by temperature changes. Hui et al. [25], by means of FEM analysis, obtained the stress and

deformation of the tunnel tube due to accidental load. Long et al. [26] revealed the effects of structure parameters of BWR, structure dump and tether stiffness on the dynamic response of SFT subjected to hydrodynamic loadings. Mai et al. [27, 28] investigated the dynamic response of SFT structure under water wave and current loadings, and also estimated the cross vibration of tether due to VIV. They found that the incident angle of wave, surface flow velocity, shape of tunnel section and support structures may affect the dynamic response of SFT, and the frequency of parametric excitation has significant influence on VIV of tension legs. Sun et al. [29-31] also investigated the effect of parameter excitation on tether VIV. They indicated that the decrease of the inclined angle and tether tension may increase the maximum vibration amplitude, and decrease the first-order natural frequency, the current velocity with regard to lock-in occurrence and the parametric excitation frequency corresponding to the maximum response.

In the following of this paper, the research advances on dynamical response and structural integrity of SFT subjected to hydrodynamic load and accidental load accomplished by our team in recent years are briefly described. Such research activities are of two aspects. One is focused on the scientific and technological issues for SFT and the other is on the design of the Archimedes Bridge Prototype (ABP) in Qiandao Lake. These are described in seven parts: (1) ABB Selection and its environmental & geotechnical conditions for ABP design, (2) Dynamic characteristics of SFT due to wave and current loads, (3) Effects of SFT structural parameters on its dynamic response, (4) Geotechnical investigations and tension pile analysis, (5) Dynamic response of SFT due to seismic load and accidental load, (6) Effects of water and sea-water on high-cycle and very-high-cycle fatigue behavior for metallic materials, and (7) Design of ABP of Qiandao Lake and its structure analysis & strength assessment.

## 2. ABB selection and its environmental & geotechnical conditions for ABP design [14]

Before the initiation of SIJLAB, the Chinese team had carried out preliminary activities for the implementation of SFT in Qiandao Lake, which was promoted by the ingenious idea of CAS President Lu Yongxiang. In August 2003, we visited Qiandao Lake, making a first time field survey of potential sites for SFT. Then, we made the preliminary field investigation of potential sites for the SFT construction in Qiandao Lake.

In November 2004, we met with local officials in Beijing, reviewing the progress of field investigation of potential construction sites and the relevant researches. Scientists and officials in this meeting noticed the difficulties of the approval process for such an innovative engineering structure without existed design codes and standards. For this situation, we proposed to build an Archimedes Bridge Prototype (ABP) in Qiandao Lake instead of one for routine tourist purpose, such that the project will have the feasibility to get approval and become a demonstrator. The local officials were definitely in favour of this new initiative.

To develop this new consideration, we further visited Qiandao Lake in March 2005, with the help of local government, searching for an appropriate site for the construction of ABP as shown in Fig. 1(b). After investigating a number of potential sites in the broad lake area, we finally made the decision of a lake bay for the location of ABP. The local authority jointly agreed with this selection. The major features of the bay are: (1) surrounded by two small peninsulas with the nearest cross width of 110m and the cross width at the two peninsula tips of 163m (at the water level with respect to the altitude of 100m), (2) adjacent to the high way connecting Qiandao Lake and Hangzhou City, and (3) the deepest water depth being 35m. On August 21, 2006, during the further field investigation of ABP location in Qiandao Lake, we imaginatively proposed an exciting name of Archimedes Bridge Bay (ABB) for the ABP location in Qiandao Lake. This has been officially endorsed by the local authority.

Based on the field survey and relevant investigations, the parameters of environmental and geotechnical conditions of ABB, including hydrological parameters, geological parameters, seismic parameters and accidental load were proposed [14], which have been used in the design and the research of ABP within SIJLAB.

It is evident that, the selection of ABB and the definition of design parameters as shown in the following are the premise and the first step of the structural design of ABP in Qiandao Lake.

### *2.1. Hydrological parameters for ABP design*

(a) Water level – maximum level: 103m, minimum level: 95m, and minimum clearance between water surface and tunnel top: 2m.
(b) Surface water wave – maximum wave height: 1m, and wave period: 1.8±0.5s.
(c) Water current – maximum water current velocity: 0.1m/s.

(d) Air temperature – average air temperature: 17.5ºC, and maximum difference of air temperature: 40ºC.
(e) Water temperature – average water temperature (water surface): 21.4ºC, and maximum difference of water temperature (surface): 20ºC.

### *2.2. Geological condition for ABP design*

The lakebed of ABB is mainly composed of tuff-sandstone randomly covered with thin soils. The medium weathered tuff-sandstone, whose compressive strength is approximately in the range from 15 to 47MPa. So that it could be served for supporting the foundations.

### *2.3. Earthquake parameters for ABP design*

Qiandao Lake area belongs to the region of earthquake intensity less than Grade 6. According to "Code for Seismic Design of Buildings" (Chinese Standard GB50011-2001) [32], the earthquake intensity for the design is taken as Grade 6, and for important buildings the intensity should be increased by one grade. Thus it is proposed the earthquake intensity for the ABP design be Grade 7. The basic acceleration corresponding to the earthquake intensity of Grade 7 is 0.1g (0.98m/s$^2$) in usual case and 0.2g (1.96m/s$^2$) in unusual case, respectively.

When time-history method is used to evaluate the response of the prototype suffered to the most serious earthquake, the maximum acceleration is 2.2m/s$^2$ in usual case and 3.2m/s$^2$ in unusual case, respectively.

### *2.4. Accidental load*

With respect to the impact of sinking boat, boat mass is estimated as 50t and impact velocity is estimated as 1m/s.

## 3. Dynamic characteristics of SFT due to water wave and current loads

SFT is submerged under water surface, and fluid-structure interaction is a basic feature of SFT dynamic response. Due to the aspect ratio (length to diameter) for integrated tunnel tube or tether is usually as large as the order of magnitude of $10^2$ to $10^3$, the slenderness of structure is necessary to be taken into account.

### *3.1. Vortex-induced vibrations of SFT structure [17, 19, 20, 33-37]*

When fluid passes a tether, vortexes form behind the tether due to fluid viscosity. Vortexes are shed periodically from fluid-structure interface. The variety of pressure on the tether surface induces the fluid forces acting on the tether along the current direction (in-line) and perpendicular to the current and tether (cross-flow). Therefore, the tether undergoes vibration induced by vortex shedding. Vortex-induced vibration (VIV) is one of the most important factors responsible for tether fatigue damage.

Wake oscillator model has been widely used in the simulation of the VIV. It is a semi-empirical formula as Eq.(1) containing two parameters $\varepsilon$ and $A$, which are deduced by experimental results. Usually, these two parameters are treated as constants.

$$\ddot{q} + \varepsilon\left(q^2 - 1\right)\dot{q} + q = A\ddot{y} \tag{1}$$

where $q$ represents non-dimensional fluid variable, $y$ is the non-dimensional tether displacement, $\varepsilon$ and $A$ are related to structural damping, mass ratio, frequency ratio, etc.

Based on the experimental results of forced oscillation cylinder, we obtained the fitted value of parameter $A$, which depends on the non-dimensional variable $\omega$ (the ratio of vortex shedding frequency to structure natural frequency). When $0 \le \omega \le 1$ is satisfied, $A$ equals 10, and if $\omega$ is larger than 1, $A$ equals 4.

According to the Skop-Griffin plot deduced by wake oscillator model, we deduced the value of $\varepsilon$, which is not a constant, but is a function of structural intrinsic characteristics. To verify the influence of $\varepsilon$ and $A$ on the structure vibration, we compared the simulation results with experimental data and the results calculated by Facchinetti et al.

[38]. Fig. 2 shows that using the variable parameters $\varepsilon$ and $A$ instead of treated as constants, the present results are better in agreement with the experimental data.

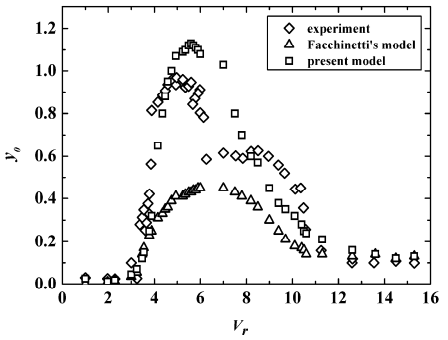


Fig. 2. Vibration amplitude as a function of reduced velocity for an elastically supported rigid cylinder [33]

Regarding the dynamic response of tether, the results of Fig.3 were obtained, showing the cross-flow vibration amplitudes for each excited modes of the tether with different inclined angles and axial pretensions. It is obvious that as the incline angle increases from zero degree, the amplitudes of the 2nd and 3rd excited mode increase first then decrease. There is an incline angle of tether corresponding to the maximum amplitude. The influence of pretension on the vibration amplitude is not similar for different excited modes. However, the total amplitude reaches the minimum when the pretension increases to a certain value.

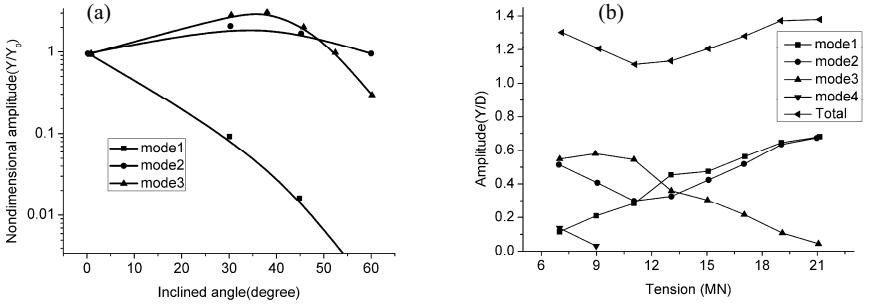


Fig. 3. (a) Vibration amplitude versus incline angle; (b) vibration amplitude versus axial pretension [36]

For the case of large aspect ratio of tether, three-dimensional vibration model is necessary in the analysis. Thus, a Cartesian right-hand coordinate system is defined with $x$ and $y$ perpendicular to the tether axis and the dynamic equation of tether is proposed as

$$\bar{m}\frac{\partial^2 \mathbf{r}}{\partial t^2}+\left(C+C'\right)\frac{\partial \mathbf{r}}{\partial t}+EI\frac{\partial^4 \mathbf{r}}{\partial z^4}-T\frac{\partial^2 \mathbf{r}}{\partial z^2}=\mathbf{F} \qquad (2)$$

where, $\bar{m}$ is the mass per unit length including fluid added mass, $C$ and $C'$ are the damping coefficients due to structure and hydrodynamic forces, $EI$ is the bending stiffness of tether, $T$ is the axial tension force in tether, $\mathbf{r}$ denotes the deflection of tether and $\mathbf{F}$ denotes the fluid forces.

The experimental data of a long riser with large aspect ratio (1400) were adopted to verify the presented model [20]. Fig. 4 shows that the simulation results of vibration frequency and dominant mode number are in good agreement with the experimental data. Moreover, it is noted that the lock-in phenomenon does not occur in the vibration of large aspect ratio riser. The vibration frequency increases linearly with current speed. The variation of dominant vibration mode number with current speed presents a step-wise pattern. It means that when the mode number does not increase with current speed, travelling wave occurs and propagates along the riser. Due to the

boundary constraints, near the ends of riser, the vibration is dominated by standing waves. As far away from the riser end, travelling wave becomes dominant. As a whole, the process of dynamic response is a combination of standing wave and travelling wave oscillations. Therefore, the frequency and the dominant mode of VIV for large aspect ratio cylinder are different from that of VIV for small aspect ratio cylinder.

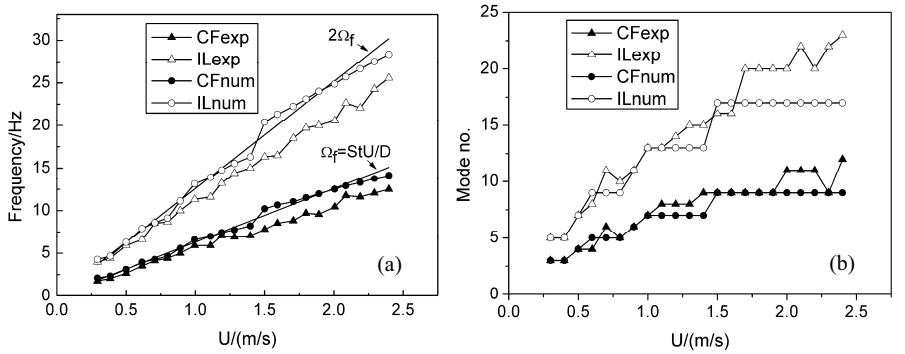


Fig. 4. (a) Frequency and (b) dominant mode of riser vibration versus current speed [20]

### *3.2. Hydroelasticity of SFT under wave condition [39-41]*

Wave propagation is always coupled with SFT motion. Due to the elasticity of SFT, the deflection and the motion of the structure may induce the radiation wave propagating. Fluid added mass and hydrodynamic damp are necessary to be taken into account in the analysis, which are the functions of structural acceleration and velocity. We adopted boundary element and structural mode decomposition methods to solve radiation wave potentials, and the dynamic equation was solved in frequency domain. As a case study, we simulated the response of ABP in Qiandao Lake due to wave forces using hydro-elastic analysis method. By considering the different types of tunnel end connectors, the distribution of tunnel deflection and axial forces at connectors are compared [41]. Under the wave condition of Qiandao Lake, the deflections of ABP are only at the order of several millimeters whether stress relaxation device is used in tunnel end connectors or not. If only one stress relaxation device is used in either tunnel end connector, the maximum axial force occurs at the other end connector. However, if stress relaxation device is used in both tunnel end connectors, axial forces will increase at every tube segment joint.

## 4. Effects of SFT structural parameters on its dynamic response

The decision of structural parameters of SFT is an essential issue in its design. Based on the fluid dynamic environment of Qiandao Lake and the structural designs of ABP proposed by SIJLAB [13, 14], the effects of structural parameters on dynamic responses of SFT under hydrodynamic loads were investigated.

### *4.1. Effect of BWR on SFT dynamic response*

Buoyancy-weight-ratio (BWR) determines the tension force in the tether section and influences the dynamic behaviour of SFT structure. The simulation results demonstrate the BWR effect on SFT dynamic responses due to hydrodynamic loads. As shown in Fig.5(a), the dynamic response in the current direction increases with the increasing of BWR. Fig. 5(b) shows that, when BWR is between 1.1 and 1.2, the vertical response decreases dramatically with the increase in BWR. When BWR continues to increase, the vertical response decreases very slowly. Note that in Figs.5-7, STDEV is the standard deviation of tunnel displacement (or amplitude of tunnel vibration) and *D* is the tunnel diameter.

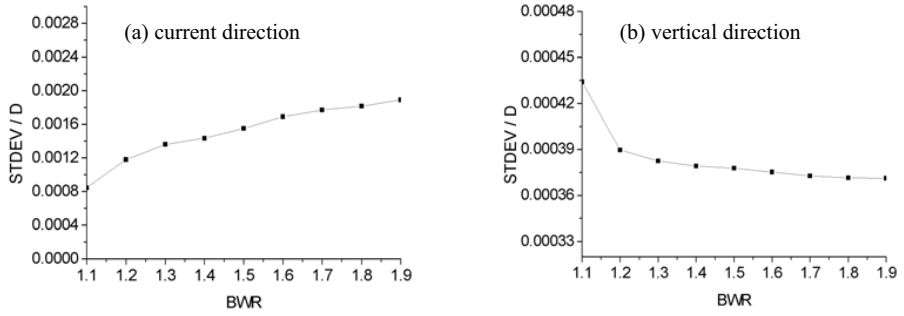


Fig. 5. STDEV at SFT mid-span under different BWRs, (a) current direction; (b) vertical direction [26]

### *4.2. Effect of tunnel outer diameter on SFT dynamic response*

The influence of tunnel outer diameter was analyzed in terms of the ratio of the net buoyancy of unit tunnel segment (100m) to the stiffness coefficient of the tether systems (BCR). Fig. 6 indicates that the dynamic response in the current direction increases as tunnel outer diameter (or BCR increases) increases, whereas in the vertical direction, the dynamic response increases as the outer diameter of tunnel segment decreases (or BCR decreases).

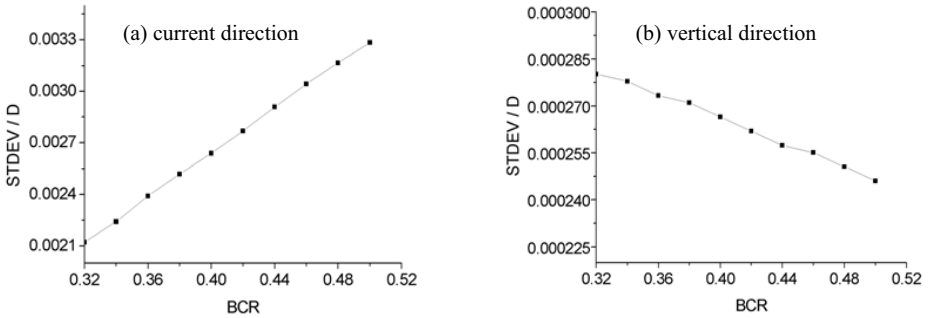


Fig. 6. STDEV versus BCR (a) current direction; (b) vertical direction [26]

### *4.3. Effect of tether system stiffness on SFT dynamic response*

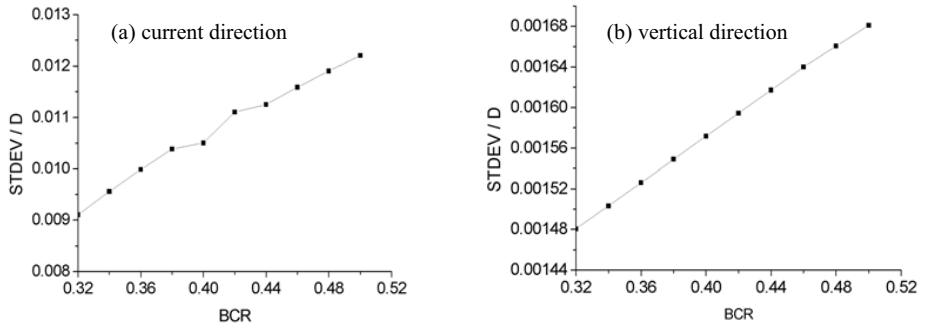


Fig.7. STDEV versus BCR, (a) current direction; (b) vertical direction [26]

The effect of tether system stiffness on the dynamic response of SFT was also examined in terms of BCR. Fig. 7 shows that the dynamic responses in both current direction and vertical direction increase as the tether system stiffness decreases (or BCR increases).

It is certain that both net buoyancy and tether stiffness are essential factors with regard to SFT stability. However, by comparison of Figs. 6(b) and 7(b), it is judged that BCR is not a characteristic factor with respect to SFT dynamics, although it is a dimensionless parameter.

### *4.4. SFT model experiment under different BWR values and tether angles*

An experiment was performed in a water tank with the size of 3.6m×1.8m×1.1m. A spherical object was released 1.13m above the water surface to impact on the water, thus to generate water wave on one side of the tank. The average wave period is 0.48s and the average wave height is 37mm. The effects of BWR and tether angle on SFT dynamic responses are given in Fig. 8. When the tube is constrained by inclined tethers, the horizontal response amplitude of the tube almost increases with the increase of BWR, whereas the vertical response amplitude of the tube decreases first, then increases and finally tends to stable [Fig. 8(a)]. The vertical response amplitude of the tube reaches the minimum when BWR approaching 1.2. Fig. 8(b) illustrates the dynamic responses of SFT when tether angle is 0°, showing the horizontal displacement is remarkably greater than the vertical displacement.

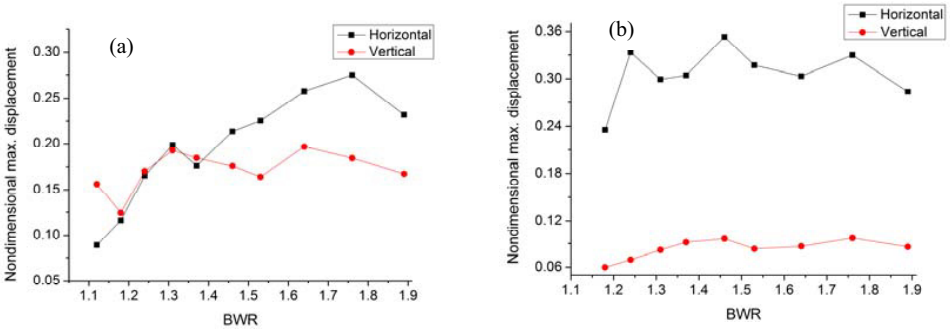


Fig. 8. SFT dynamic response versus BWR under (a) tether angle of 30°; (b) tether angle of 0° [42]

Our both theoretical simulations and experiments indicate that BWR dominates the dynamic response of SFT and is the most important parameter to be considered in SFT structural design. For this, we propose the concept of "Synergetic range of BWR". This is defined as, for an SFT structure with related environmental conditions, there exists a suitable range of BWR value which will lead to less dynamic response and more stability for the SFT. For ABP in Qiandao Lake, the Synergetic range of BWR is between 1.2 and 1.3.

### *4.5. Effect of tether angle on dynamic tension of SFT tethers*

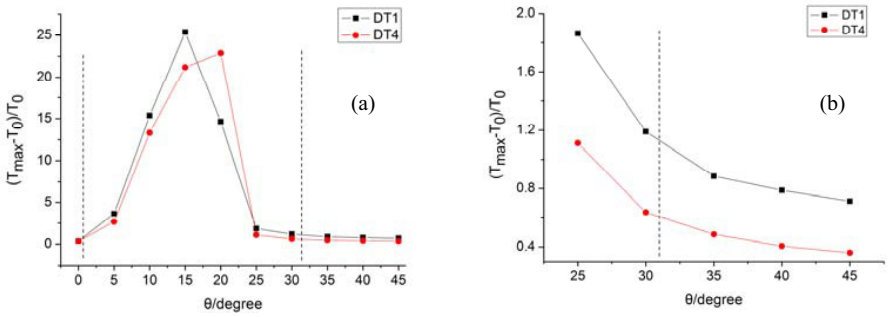


Fig. 9. (a) Relative dynamic tension versus tether angle; (b) enlargement of (a) for $\theta \geq 25^{\circ}$ [42]

In addition, the slacking phenomenon was investigated, and the conceptual design of SFT for Funka Bay with a span of 30km and a depth of 100m was taken as the analysis case. As an example, Fig. 9(a) shows the relation between relative dynamic tension and tether angle $\theta$, and Fig. 9(b) is the enlargement of right part of Fig. 9(a) for $\theta \geqslant 25^{\circ}$. It is seen that the relative dynamic tension increases sharply with $\theta$ first, and then decreases. If $\theta$ is larger than 30º, the response becomes stable. The relative dynamic tension reaches its peak value around the tether angle of 15º. This tendency should be considered in relevant SFT design.

## 5. Geotechnical investigations and tension pile analysis [14, 43, 44]

Based on the geotechnical analyses of the sediment samples at the five boring and sampling positions, the engineering geology section was obtained. There usually exist five layers along the selected route along the lakebed, i.e. silt, silty clay, gravel mixed with silty clay, highly-weathered tuff-sandstone, and medium weathered tuff-sandstone. The silt and gravel layers may be missing at some locations. The lakebed is a kind of layered sediment, which is mainly composed of tuff-sandstone covered with thin soils. The medium weathered tuff-sandstone has excellent bearing capacity and no faults or crash zones have been detected in this stratum. The lakebed is characterized with deep sloping surface, thus the tension pile is considered as the potential foundation solution for ABP.

The uplift bearing capacity of the tension pile embedded in the layered sediments was investigated numerically. In the numerical model, the parameters of the layered sediments were chosen with some reference to the properties of the sediments at Qiandao Lake. Numerical results indicate that, the sediment characteristics have much influence on the shear stress along the pile-sediment interface [Fig. 10(a)]. As the pile-top displacement increases up to a certain value, the pile-sediment interfacial shear stress at the Layer-5 (medium-weathered tuff sandstone) becomes much larger than that at the Layer-2 (clay), which indicates that the layer of medium-weathered tuff sandstone contributes much larger to the resultant uplift capacity of the tension pile than the upper soft sediment covers.

With the increase of pipe-top displacement, the uplift load increases gradually to its maximum value. For this examined layered sediment, the values of the ultimate tension load increases with the increase of the pile length [Fig. 10(b)]. Note that, a critical length of the tension piles exists under most of pile/sediment conditions. That is, the ultimate tension load would stop increasing while the pile length reaches its critical value [44].

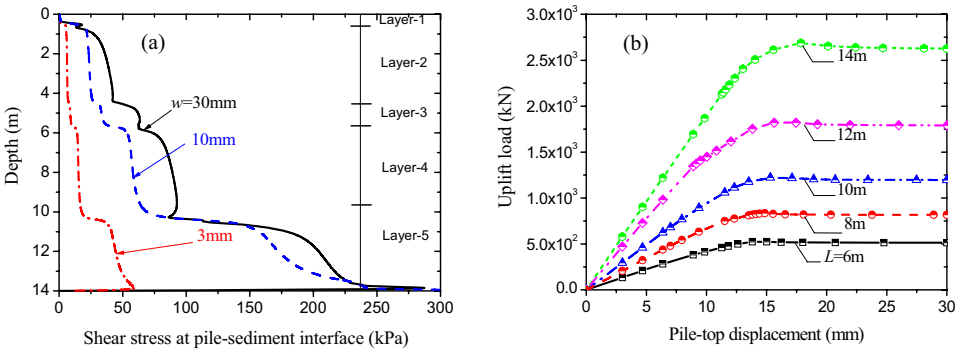


Fig. 10. (a) Development of shear stress along pile-sediment interface for various values of pile-top displacement (pile length $L$ = 14m, pile diameter $D$ = 0.6m); (b) uplift load-displacement curves of single tension pile for various values of pile length ($L$=6~14m; $D$ = 0.6m)

For the optional mooring systems of ABP, the tension piles may be either vertically loaded or obliquely loaded. Thus, the effects of loading angle on the uplift resistance of the tension pile were also investigated by employing the symmetric three-dimensional finite element model for oblique loading. The variation of the total tension load with pile-top displacement of an obliquely-loaded single tension pile is shown in Fig. 11. It is indicated that, the loading angle has much influence on the ultimate tension load. For a certain value of pile-top displacement, the oblique loads get smaller with increasing loading angle. The ultimate values of tension load tend to become larger for bigger loading angles. Nevertheless, the pile-top displacement would become the more prevailing influential factor while increasing the loading angle.

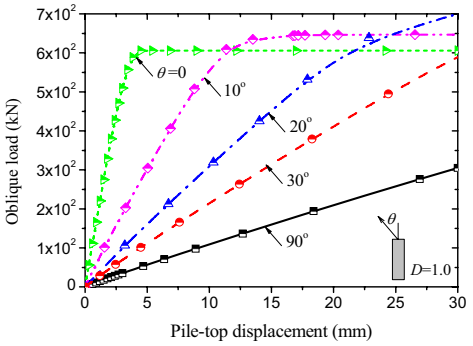


Fig. 11. Effects of loading angle on tension load development with pile-top displacement of an obliquely-loaded single tension pile

## 6. Dynamic response of SFT due to seismic load and accidental load

### *6.1. Effect of seismic load on dynamic response of SFT with various shore connections [45]*

A numerical model was developed based on the finite element method to study the dynamic response of SFT due to seismic loading. Five types of shore connections were considered for an SFT subjected to uniform seismic excitation, i.e. A: rigid connection, B: hinged connection, C: elastic bearing, D: bi-elastic bearing and E: elastic-plastic bearing. Fig. 12(a) shows the comparison of the transverse moment of SFT for the five cases of shore connections. It is seen that the seismic response, especially near the shore ends, is reduced remarkably for the cases of bi-elastic and elastoplastic bearings. This result is helpful to the aseismiatic design of SFT. In addition, a parametric analysis for the elastic, bi-elastic and elastoplastic bearings was made, which gave the quantitative relations between the amount of vibration mitigation and the parameters of bearings, such as the stiffness and yield force or turning force. This information provides a convenient reference for the design of SFT.

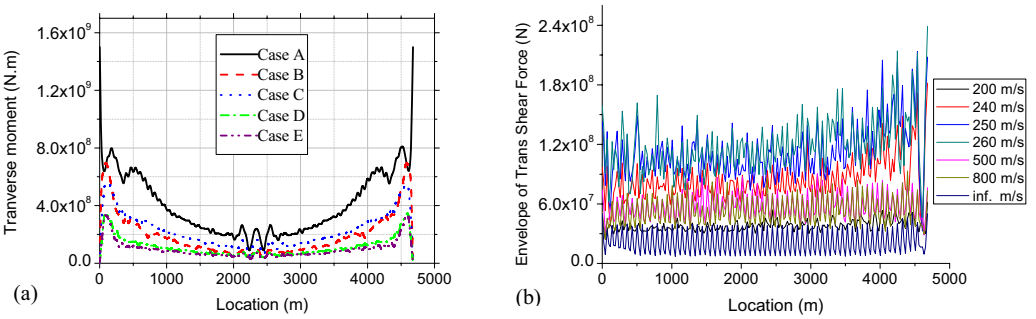


Fig. 12. (a) Seismic responses of SFT with different shore connections; (b) envelopes of transverse shear force of SFT under uniform excitation and multiple excitations with various wave velocities

### *6.2. Seismic wave passage effect [46]*

A numerical analysis was also performed to investigate the dynamic characteristics of SFT due to seismic wave passage effect. The large mass method was implemented to simulate the dynamic response of SFT subjected to multiple support seismic excitations with various wave velocities. Fig. 12(b) depicts the seismic wave passage effect with various wave velocities, where the situation of infinite velocity is equivalent to uniform excitation. It is found that the response under the multi-support excitation is much intensive than that under the uniform excitation and varies with the velocity of seismic waves in a non-monotone way. There exists a peak velocity of seismic waves,

which corresponds to the maximum response of the structure. In addition, for every velocity, the most remarkable response appears near the shore connection corresponding to the output end of the seismic wave.

Furthermore, an analytical study shows that the resonance due to the periodic hitting of seismic wave is responsible for this appreciable dynamic magnification, which is unique to long-span periodic structures, such as SFT. It is worth paying special attention to this resonance in the aseismatic design of SFT.

*6.3 Effect of accidental impact load [25]*

SFT is located under water surface. There is a potential risk of collision due to sink ship or other objects. Therefore, for the safety of SFT, it is important to analyze the structure resistance to impact load. Numerical simulation based on the ANSYS/LS_DYNA was performed to demonstrate the analytical solution. In the simulation, the length of tunnel tube is 20m, the diameter is 4m, the thickness of wall is 0.1m, the Young's modulus of shell material is $2.1\times10^5$ MPa , the density is $7800\text{kg/m}^3$ and the Poisson's ratio is 0.3. The impact object is assumed to be rigid. The object mass is set as 10 tons and the impact velocity is 3m/s.

The results showed that if the fluid added mass is considered, the radial displacement decreases and the Mises stress increases. The influence of impact velocity was also investigated. The results show that the radial displacement and Mises stress vary linearly as it increases. If the material of shell is steel Q420 with yield stress of 325MPa, when the impact velocity approaches 4.0m/s, the shell will yield at the impact position.

## 7. Effects of water and sea water on high-cycle and very-high-cycle fatigue behavior of metallic materials [47]

One of the important loading characteristics for SFT structure and related materials is that the mooring tethers and the connection joints between two segments or between tunnel and shore are subjected to high average stress (induced by structure weight, infrastructure weight and buoyancy) superimposed by cyclic loading (due to hydrodynamic load, traffic load or accidental load). If the cyclic loading frequency is of the order of magnitude of 1Hz, the total number of loading for the related structure or material will reach $10^8$ cycles after 3 years in service, which is within the very-high-cycle fatigue (VHCF) regime [48]. Moreover, such a loading situation is inevitably coupled with the effect of water or sea water environment. Thus, the high-cycle and VHCF fatigue behaviour in water or sea water for related materials is an essential aspect for SFT structure integrity. And there is still a lack of investigations regarding the effect of environmental medium on VHCF behaviour of high strength metallic materials.

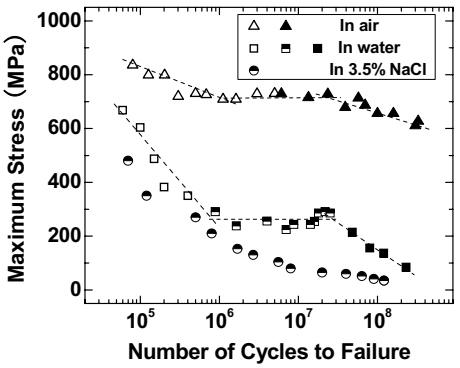


Fig. 13. S-N curves tested in air, water and sea water, hollow: surface crack origination, solid: subsurface origination, and semi-solid: mixed mode

The material tested in this investigation was a structural steel (0.4%C, 1%Cr). Hour-glass shape specimens were used with the minimum diameter of 3mm. The ultimate tensile strength of the specimen was 1582MPa. Fatigue tests were performed by using a rotary bending machine at room temperature, operated at the frequency of 52.5 Hz, and with the stress ratio of −1. Three types of test environmental media were adopted: laboratory air, fresh water and 3.5% NaCl aqueous solution (sea water). For further examination of fatigue crack propagation in sea water, hour-glass type specimens with V-notch at reduced section were also tested.

The results of S-N curves for specimens tested in laboratory air, water and sea water are shown in Fig. 13. For fatigue testing in water, a stepwise S-N curve presents (squares in Fig. 13), but the maximum stress value, i.e. fatigue strength, of transition part in the S-N curve is dramatically decreased, which (260MPa) is only 36% of that in laboratory air testing (720MPa). In VHCF regime, the difference of fatigue strength between the two cases is even larger. For fatigue testing in sea water, the S-N curve (circulars in Fig. 13) exhibits a continuously descending shape. The fatigue strength is even lower than that tested in water.

The fatigue strength in aqueous solutions is substantially degraded and the reduction increases gradually with decreasing stress level. The ratio of fatigue strength tested in water to that tested in air at the failure life of $10^7$ is 34%. This ratio decreases to 21% at $10^8$ failure cycles. Furthermore, the ratio of fatigue strength tested in sea water to that tested in air is only 10% at $10^7$ cycles, and is even lower of 5.8% at $10^8$ cycles. The above description is expressed as:

$$\left.\frac{\sigma_{\max}^{w}}{\sigma_{\max}^{a}}\right|_{10^7} = 0.34 \qquad \left.\frac{\sigma_{\max}^{w}}{\sigma_{\max}^{a}}\right|_{10^8} = 0.21 \tag{3}$$

and

$$\left.\frac{\sigma_{\max}^{s}}{\sigma_{\max}^{a}}\right|_{10^7} = 0.10 \qquad \left.\frac{\sigma_{\max}^{s}}{\sigma_{\max}^{a}}\right|_{10^8} = 0.058 \tag{4}$$

where $\sigma_{\max}^{w}$ is the fatigue strength tested in water, $\sigma_{\max}^{s}$ is that in sea water and $\sigma_{\max}^{a}$ is that in laboratory air. The severe degradation of fatigue strength for metallic materials in water and sea water in high-cycle and VHCF regimes should be paid enough attention in strength design, material selection and life estimation of SFT.

The observations on V-notch specimens cyclically loaded in sea water showed that multiple crack origins prevailed at specimen surface or subsurface covering almost the circumference of the notch root, and that a large portion of fracture surface resulted from corrosion fatigue cracking. The cracking area fraction gradually increased with the number of loading cycles.

Under aqueous environment, the failure mechanism of high strength steel has been confirmed as hydrogen induced embrittlement. In the present investigation of fatigue behavior in the test environments of water and sea water for the structural steel, the typical phenomena were: multiple crack origins, surface cracking associated with subsurface micro-voids for crack initiation and early growth, and intergranular cracking morphology with widespread secondary intergranular cracks, which are evidences of hydrogen induced damage due to the effect of aqueous solution. In the process of hydrogen induced damage and failure, the diffusion and concentration of hydrogen is proportional to time variable $t$ [49]: $X_d = 4\sqrt{D_H t}$ , where $X_d$ is the maximum depth of hydrogen penetration and $D_H$ is the hydrogen diffusion coefficient of $10^{-5}$ mm$^2$/s [50]. Such that we obtained the variation tendency of $X_d$ versus $t$, i.e. the number of loading cycles, by taking $t = N / f$ with $f$ being the cycling frequency of 52.5Hz. The results show the increasing tendency of hydrogen penetration with time variable. Thus, one may anticipate that a large time period for a specimen exposed to aqueous environment while cyclic loading will lead to larger value of hydrogen diffusion depth into the specimen and therefore more extensively corrosive effect of environment superimposed on the mechanical loading, which is the qualitative explanation for the cracking area increasing with loading cycles and for the large difference of fatigue strength between the cases tested in air and in aqueous solutions at higher failure lives, i.e. the fatigue strength is inversely proportional to fatigue failure cycles when introducing aqueous environment, as shown in Fig. 13.

## 8. Design of ABP of Qiandao Lake and its structure analysis & strength assessment [13, 14, 51, 52]

As mentioned in Introduction, we have searched and decided the ABB for the construction of ABP in Qiandao Lake. The crossing length of the selected route for ABP is 117 meters, and ABP is divided into 5 segments (modules). For the cross section of ABP, a circular shape has been proposed [13], which is composed by three shells: inside a steel tube (0.02m), in the middle a reinforced concrete one (0.30m), and the outside an aluminum one (0.10m). Thus, the total thickness of the sandwich wall is 0.42m.

### 8.1. BWR, effective density and deformation stiffness of homogenized shell

By homogenizing the three-layered composite shell to a single-layer shell while keeping the effective stiffness, the mass as well as the inner and the outer diameters constant, then BWR, effective density and deformation stiffness of homogenized shell were obtained. The values of BWR for the tube, the tube with infrastructure and the tube with infrastructure and live load are calculated as 1.320, 1.215 and 1.140, respectively. Referred to Section 3, the Synergetic range of BWR for ABP is between 1.2 and 1.3. Note that the BWR for the tube with infrastructure and live load is only 1.140, which is relatively small. Therefore, the adjustment of the ABP cross section should be considered.

The effective density is $2.19\times10^3$ kg/m$^3$. Based on the equivalence principle of stiffness, the effective compressive stiffness and bending stiffness are $18.86\times10^{10}$N and $33.5\times10^{10}\mathrm{N}\cdot\mathrm{m}^2$, respectively.

### 8.2. Deformation stress and strength assessment of ABP tube

When the aspect ratio (length to diameter) of tube is greater than 5, the shear deformation is relatively small and consequently, the planar cross-section deformation assumption can be used. According to the data of hydrodynamic load, seismic load and accidental load in the design report [14], the values of the maximum stress for ABP tube were calculated. The data in Table 1 indicate that the maximum stress under seismic loading is the largest. The maximum stress due to seismic induced tension is much greater than the strength of materials used in ABP. This should be considered in the revision of the design.

Table 1. Data of the maximum stress of ABP tube

| | Wave loading | Seismic induced tension | Seismic induced bending | Accidental loading |
|---|---|---|---|---|
| Maximum stress | 3.88 MPa | 3.06GPa (for steel)<br>0.187GPa (for concrete) | 24.6MPa | 17.1MPa |

### 8.3. Stress of connecting bolts

144 bolts are used to connect two modules for the prototype, which are distributed along a circular line of 3.27m in diameter. The diameter of the bolt is 30mm. According to hydrodynamic load, seismic load in design report [14], the maximum stress of bolts was calculated. The data in Table 2 show that the bolt stress under seismic bending load is the largest. The strength of material (410.3MPa) does not meet such extreme condition.

Table 2. Data of bolt stress

| | Wave & current loading | Seismic induced tension | Seismic induced bending | Seismic shearing |
|---|---|---|---|---|
| Bolt stress, MPa | 94.58 | 23.58 | 626.2 | 27.0 |

### 8.4. Natural frequencies of ABP

ABP is anchored to the lake foundation by steel tethers, which give significant influence to the vibration behaviour of ABP. Here the transversal natural frequencies of ABP without added mass and live load, with added mass, and with added mass and overload are listed in Table 3. It should be pointed out that in the calculation of the transversal vibration frequencies, the supporting effect of tethers was ignored.

Table 3. Data of transversal natural frequencies of ABP

| Support condition | Frequency, Hz | Frequency, Hz (with added mass) | Frequency, Hz (with overload & added mass) |
|---|---|---|---|
| Simply-simply | 2.72 | 1.78 | 1.72 |
| Fixed-fixed | 5.25 | 3.47 | 3.35 |

*8.5. Deformation of ABP under accidental impact load and estimation of energy absorption of aluminum panel*

Table 4 and Table 5 list the data of energy absorption for ABP. It is evident that the aluminum alveolate layer has considerable capacity in absorbing accidental collision energy. For this particular case, the energy absorbed is larger than 80% of the impacting energy.

Table 4. Deformation and stress of ABP due to impact load

| | Without added mass | With added mass |
|---|---|---|
| Deflection, mm | 6.34 | 5.57 |
| Mises stress, MPa | 41.4 | 46.0 |

Table 5. Energy absorption of ABP due to impact load

| | Total impact energy | energy absorption by skin | Energy absorption by webs | Total energy absorption |
|---|---|---|---|---|
| Energy, J | $2.5\times10^4$ | $1.88\times10^4$ | $0.21\times10^4$ | $2.1\times10^4$ |

## 9. Concluding remarks

The creative results on dynamic response and structural integrity of SFT due to hydrodynamic load and accidental load obtained by our team have been summarized with the following main remarks.

(1) The location of ABP has been determined and the related design parameters have been defined, which are the premise for the design and the research of ABP within SIJLAB.

(2) The distinct characteristics of VIV for SFT structure with large aspect ratio are revealed: vibration without lock-in phenomenon, vibration frequency increasing linearly with current speed, and the combination of standing wave and travelling wave oscillations.

(3) The concept of "Synergetic range of BWR" is proposed. For ABP in Qiandao Lake, the Synergetic range of BWR is between 1.2 and 1.3.

(4) The uplift capacity of tension pile with regard to ABB foundation is solved, showing the possibility of the tension pile solution.

(5) Seismic effect on SFT is significant, and the response caused by seismic wave passage effect is several folds larger than that due to uniform excitation.

(6) The fatigue strength of steel in sea water for $10^8$ cycles is only 5.8% of that in air environment. Such severe degradation should be paid enough attention in the strength design of SFT.

(7) The strength assessment for ABP shows the previous design should be revised to improve the safety and reliability of the Prototype.

These achievements provide the scientific and technological principles for SFT realization in Qiandao Lake and in the world.

## Acknowledgements

This paper is supported by National Natural Science Foundation of China (nos. 10532070, 10772178) and Knowledge Innovation Program of Chinese Academy of Sciences (no. KJCX2-YW-L07). The authors express their appreciations to Prof. Shuangyin Zhang, Prof. Fuping Gao, Prof. Guojun Huang, Prof. Weimin Chen, Mr. Xiaodong Wu and Mr. Wei Lu for their assistance in the preparation of this paper.

## References

[1] Brancaleoni F, Castellani A, D'Asdia P. The response of submerged tunnels to their environment. *Engng Struct* 1989; 11: 47-56.

[2] Remseth S, Leira BJ, Okstad KM, Mathisen KM, Haukas T. Dynamic response and fluid/structure interaction of submerged floating

tunnels. *Computers and Structures* 1999; 72: 659-85.

[3] Kanie S, Kokubun H, Mizutani Y, Mikami T, Kakuta Y. Analytical study on dynamic response of submerged floating tunnels due to wave force. *Proc. 3rd Symp on Strait Crossings*, Alesund, Norway; 1994, p.659-66.

[4] Kunisu H, Mizuno S, Mizuno Y, Yamashita T, Saeki H. Numerical analysis of wave force and dynamic response to the submerged floating tunnels. *Proc 3rd Symp on Strait Crossings*, Alesund, Norway; 1994, p.637-44.

[5] Kunisu H, Mizuno S, Mizuno Y, Saeki H. Study on submerged floating tunnel characteristics under the wave condition. *Proc Fourth Int Offshore Polar Engng Conf*, Osaka, Japan; 1994, p.27-32.

[6] Fogazzi P, Perotti F. The dynamic response of seabed anchored floating tunnels under seismic excitation. *Earthquake Engng and Struct. Dynamics*, 2000; 29: 273-95.

[7] Di Pilato M, Perotti F, Fogazzi P. 3D dynamic response of submerged floating tunnels under seismic and hydrodynamic excitation. *Engng Struct* 2008; 30: 268-81.

[8] Kiyokawa K, Inada Y. Analysis of hydrodynamic force acting on submerged structures during earthquakes. *Proc Coastal Engng Japan* 1990; 37: 639-43.

[9] Morita S, Mizuno Y, Mineta M, Kurosaki K. Earthquake response analysis of submerged floating tunnels considering water compressibility. *Proc Forth Int Offshore Polar Engng Conf*, Osaka, Japan; 1994, p.20-6.

[10] Venkataramana K, Yoshihara S, Toyoda S, Aikou Y. Current-induced vibrations of submerged floating tunnels. *Proc Sixth Int Offshore Polar Engng Conf*, Los Angels, USA; 1996, p.111-8.

[11] Xiang Y, Gan Y, Xu X. Report on spatial analysis of the submerged floating tunnel in the Jintang strait. *Sino-Italian Protocol on Scientific and Technological Cooperation – Technical Feasibility Study Project of the Submerged Floating Tunnel in the Jintang Strait*, 2003.

[12] Li J, Li Y. Analytical solution to the vortex-excited vibration of tether in the submerged floating tunnel. *Underground Construction and Ground Movement*, ASCE 2006: 164-169.

[13] Fiorentino A, Mazzolani FM, Perotti F, et al. (Italian Team of SIJLAB). Design report of the Archimede's bridge prototype in Qiandao Lake (P.R of China). Italy. 2007.

[14] Hong Y, Li J. Liang N, Ge F, Huang G, Gao F, Lin M, Chen W, Zhang S, Wu Y, et al. (Chinese Team of SIJLAB). Report of research and design for Archimedes bridge prototype at Qiandao Lake, Institute of Mechanics, CAS, 2007.

[15] Ling D, Zhang J, Xiang Y, Xu X. The method of virtual laminated element and its application in bridge engineering. *China Civil Engng J* 1998; 31(3): 22-9. (in Chinese)

[16] Xiang Y, Gan Y, Xu X. Spatial analysis of the submerged floating tunnel in the Jintang strait. *Seventh Int Symp on Struct Engng for Young Experts*, 2002, Tianjin, China.

[17] Ge F, Dong M, Hui L, Hong Y. Vortex-induced vibration of submerged floating tunnel tethers under wave and current effects. *Engng Mech* 2006; 23(S): 217-21. (in Chinese)

[18] Ge F, Hui L, Hong Y. Research on nonlinear vortex-induced vibrations of submerged floating tunnel tethers. *China J Highway Transport* 2007, 20(6): 85-9. (In Chinese)

[19] Ge F, Hui L, Hong Y. Vortex-induced vibration of submerged floating tunnel tethers in shear current. *J Graduate School Chinese Academy of Sciences* 2007; 24(3):351-6. (in Chinese)

[20] Ge F, Long X, Wang L, Hong Y. Flow-induced vibrations of long circular cylinders modeled by coupled nonlinear oscillators. *Sci China, Series G - Phy Mech & Astronomy* 2009; 52: 1086-93.

[21] Chen W, Wang Y. Effect of tension and flow distribution to vortex-induced vibration response of tension leg. *Shipbuilding of China* 2004; 45(S): 226-32. (in Chinese)

[22] Wang Y, Chen W, Lin M. The added mass in the lock-in range and its influence to vortex-induced vibration. *Shipbuilding of China* 2006; 47(S):170-8. (in Chinese)

[23] Dong M, Ge F, Zhang S, Hong Y. Dynamic equations for curved submerged floating tunnel. *Appl Math Mech* 2007; 28: 1299-308.

[24] Dong M, Ge F, Hong Y. Analysis of thermal internal forces for curved submerged floating tunnels. Engng Mech, 2006, 23(S): 21-4. (in Chinese)

[25] Hui L, Ge F, Hong Y. Calculation model and numerical simulation of submerged floating tunnel subjected to impact loading. *Engng Mech* 2008, 25(2): 209-13. (in Chinese)

[26] Long X, Ge F, Wang L, Hong Y. Effects of fundamental structure parameters on dynamic responses of submerged floating tunnel under hydrodynamic loads. *Acta Mech Sinica* 2009; 25: 335-44.

[27] Mai J, Yang X, Guan B. Dynamic response analysis of the submerged floating tunnel subjected to the wave and current. *J Hydrodynamics* 2005; 20(5): 616-23. (in Chinese)

[28] Mai J, Luo Z, Guan B. Vortex-induced dynamic response of tension legs for submerged floating tunnel under current effect. *J Southwest Jiaotong University* 2004; 39(5): 600-4. (in Chinese)

[29] Sun S, Chen J. Multi-order vortex-induced nonlinear vibration of submerged floating tunnel tether. *J Dalian Maritime University* 2007; 33(4): 86-90. (in Chinese)

[30] Sun S, Chen J, Su Z. Study on nonlinear parametric vibration of a tether-tube coupled and submerged floating tunnel. *J Vibration Shock* 2007; 26(10): 104-8. (in Chinese)

[31] Chen J, Wang B, Sun S. Analysis of vortex-induced dynamic response for the anchor cable of submerged floating tunnel. *Engng Mech* 2007; 24(10): 186-92. (in Chinese)

[32] Code for Seismic Design of Buildings (GB50011-2001), Issued on July 20, 2001, National Standard of China. (In Chinese)

[33] Xu W, Zeng X, Wu Y. High aspect ratio (L/D) riser VIV prediction using wake-oscillator model. *Ocean Enging* 2008; 35: 1769-74.

[34] Xu W, Wu Y, Zeng X. A new wake oscillator model for predicting vortex induced vibration of a circular cylinder. *J Hydrodynamics* 2010. (in press).

[35] Wang Y, Chen W, Lin M. Study on the variation of added mass and its application to the calculation of amplitude response for a circular cylinder at lock-in. *China Ocean Engng* 2007; 21(3): 429-37.

[36] Chen W, Zhang L, Li M. Prediction of vortex-induced vibration of flexible riser using improved wake-oscillator model. *Engng Mech* 2010; 27(5): 240-6. (in Chinese)

[37] Ge F, Long X, Wang L, Hong Y. Study of vortex-induced vibration of submerged floating tunnel tube-tether coupled model. *China J Highway Transport* 2009; 22(3): 83-8. (in Chinese)

[38] Facchinetti ML, deLangre E, Biolley F. Coupling of structure and wake oscillators in vortex-induced vibrations. *J Fluids Struct* 2004;19: 123–40.

[39] Ge F, Hui L, Hong Y. Nonlinear response of submerged floating tunnel to wave forces. *Chinese J Appl Mech* 2008; 25(2): 207-11. (in Chinese)

[40] Ge F, Hui L, Hong Y. Research on dynamic response of submerged floating tunnel to regular wave forces. *Engng Mech* 2008; 25(6): 188-94. (in Chinese)

[41] Ge F, Lu W, Wu X, Hong Y. Fluid-structure interaction of submerged floating tunnel in wave field. *Proc 1st Int Symp Archimedes Bridge*, Qiandao Lake: Elsvier, Procedia Engineering 2010; 4: 263-71.

[42] Lu W, Ge F, Wang L, Hong Y. Dynamic response of submerged floating tunnels considering tether slacking under wave condition. Submitted.

[43] Gao F, Yan W, Ge F. Geotechnical investigation and tension-pile solution for foundation of SFT prototype at Qiandao Lake. *Proc 1st Int Symp Archimedes Bridge*, Qiandao Lake: Elsvier, Procedia Engineering 2010; 4: 127-34.

[44] Yan W, Gao, F. Numerical analysis of interfacial shear degradation effects on axial uplift capacity of a tension pile, *Proc 1st Int Symp Archimedes Bridge*, Qiandao Lake: Elsvier, Procedia Engineering 2010; 4: 273-81.

[45] Xiao J, Huang G. Transverse earthquake response and design analysis of submerged floating tunnels with various shore connections, this proceedings, *Proc 1st Int Symp Archimedes Bridge*, Qiandao Lake: Elsvier, Procedia Engineering 2010; 4: 233-42.

[46] Chen W, Huang G. Seismic wave passage effect of dynamic response of submerged floating tunnels, *Proc 1st Int Symp Archimedes Bridge*, Qiandao Lake: Elsvier, Procedia Engineering 2010; 4: 217-24.

[47] Qian G, Hong Y. Effects of environmental media on high cycle and very-high-cycle fatigue behaviors of structural steel 40Cr. *Acta Metall Sinica* 2009, 45: 1356-63. (in Chinese)

[48] Stanzl SE, Tschegg EK, Mayer H. Lifetime measurements for random loading in the very high cycle fatigue range. *Int J Fatigue* 1986; 8: 195-200.

[49] Shipilov SA. Location of the fracture process zone for hydrogen-induced corrosion fatigue crack propagation. *Scripta Mater* 2002; 47: 301-5.

[50] Page RA, Gerberich WW. The effect of hydrogen source on crack initiation in 4340 steel, *Met Trans A* 1982; 13A: 305-11.

[51] Zhang S, Wang L, Hong Y. Structural analysis and safety assessment of submerged floating tunnel prototype in Qiandao Lake. *Proc 1st Int Symp Archimedes Bridge*, Qiandao Lake: Elsvier, Procedia Engineering 2010; 4: 179-87.

[52] Zhang S, Wang L, Hong Y. Vibration behavior and response to an accidental collision of SFT prototype in Qiandao Lake. *Proc 1st Int Symp Archimedes Bridge*, Qiandao Lake: Elsvier, Procedia Engineering 2010; 4: 189-97.